Research Square

Preprints are preliminary reports that have not undergone peer review.
They should not be considered conclusive, used to inform clinical practice,
or referenced by the media as validated information.

A connectomic census of axo-axonic inhibition in Drosophila: control of nociceptors is concentrated in one body-wide inhibitor

João Pedro do Couto Caetano
joao.caetano@sou.ucpel.edu.br
Federal University of Pelotas
Juliana da Rosa Perez
Universidade Católica de Pelotas
Fátima Caroline dos Santos Welter
Universidade Católica de Pelotas
Vilson Farias Junior
Universidade Católica de Pelotas
Rodrigo Mendes Rezende
Federal University of Pelotas
Fernanda Silveira Prado
Universidade Católica de Pelotas
Lucas Damé Simões
Federal University of Pelotas
Artur Ramos Molina
Federal University of Juiz de Fora

Research Article

Keywords: Connectome, Nociception, Presynaptic inhibition, Gamma-aminobutyric acid, Drosophila melanogaster, Sensory afferents

Posted Date: November 18th, 2026

DOI: https://doi.org/10.21203/rs.3.rs-11653602/v1

License: This work is licensed under a Creative Commons Attribution 4.0 International License.
Read Full License

Additional Declarations: No competing interests reported.

A connectomic census of axo-axonic inhibition in *Drosophila*: control of nociceptors is concentrated in one body-wide inhibitor

João Pedro do Couto Caetano[1,2], Juliana da Rosa Perez[2], Fátima Caroline dos Santos Welter[2], Vilson Farias Junior[2], Rodrigo Mendes Rezende[3], Fernanda Silveira Prado[2], Lucas Damé Simões[4], Artur Ramos Molina[5]

[1] Postgraduate Program in Dentistry, School of Dentistry, Federal University of Pelotas, Pelotas, Brazil

[2] Faculty of Medicine, Universidade Católica de Pelotas, Pelotas, Brazil

[3] Center for Technological Development, Federal University of Pelotas, Pelotas, Brazil

[4] Cancer Biotechnology Laboratory, Center for Technological Development, Federal University of Pelotas, Pelotas, Brazil

[5] Postgraduate Program in Biodiversity and Nature Conservation, Federal University of Juiz de Fora, Juiz de Fora, Brazil

Corresponding author: João Pedro do Couto Caetano, e-mail: jpcaetano8@gmail.com

ORCID: João Pedro do Couto Caetano, 0009-0006-0112-6280

ORCID: Juliana da Rosa Perez, 0009-0005-4517-3524

ORCID: Fátima Caroline dos Santos Welter, 0009-0004-7688-6343

ORCID: Vilson Farias Junior, 0009-0008-2939-4345

ORCID: Artur Ramos Molina, 0000-0002-6022-6760

ORCID: Rodrigo Mendes Rezende, 0009-0006-9037-2773

ORCID: Fernanda Silveira Prado, 0009-0005-5178-2342

ORCID: Lucas Damé Simões, 0000-0001-7694-7370

Acknowledgements

The authors thank the teams that generated and openly released the male-CNS, MANC and BANC connectomes.

Abstract

Presynaptic inhibition of primary afferent terminals sets the gain of sensory transmission, yet its organisation has been described one modality at a time. All synaptic input onto every class of sensory afferent was counted in three independently acquired electron microscopy connectomes of adult *Drosophila melanogaster* (two males and one female), and the input from neurons predicted to use gamma-aminobutyric acid (GABA) was decomposed by presynaptic cell type. Inhibitory control was partitioned by modality: the three classes that terminate in the antennal lobe shared one inhibitor, recovering an experimentally established olfactory case, and each of the seven remaining classes was dominated by a different GABAergic cell type. Nociceptive multidendritic afferents had the most concentrated control of any somatosensory class in all three animals. In the complete male central nervous system, a single bilateral pair of neurons, AN05B004, supplied 57% of their total synaptic input, against 3% to 20% for the largest source onto each mechanosensory class. Each AN05B004 neuron received input from, and returned output to, all 77 nociceptors of the abdomen, legs and wings on both sides of the body, an architecture of global gain control. The partition was synaptic rather than positional, and AN05B004 synapses lay a median of 1.30 μm from the afferent release sites, against 7.32 μm expected by chance. In a network model, silencing AN05B004 raised ascending nociceptive output 3.6-fold without raising global activity. Nociceptive afferents therefore carry the least redundant inhibitory control of any somatosensory class, a prediction testable in the mammalian dorsal horn.

Keywords Connectome · Nociception · Presynaptic inhibition · Gamma-aminobutyric acid · *Drosophila melanogaster* · Sensory afferents

Introduction

The first synapse of a sensory pathway is not a passive relay. At the terminals of primary afferent neurons, inhibitory interneurons form axo-axonic contacts that scale transmitter release per spike rather than blocking the spike itself. This presynaptic inhibition expands dynamic range, suppresses reafference during self-generated movement and sets the threshold at which afferent activity recruits second-order neurons (Rudomin and Schmidt 1999; Root et al. 2008; Fernandes et al. 2020). It is among the more conserved motifs in nervous systems, appearing at primary afferent terminals in the vestibular, visual, olfactory and somatosensory systems of both invertebrates and vertebrates (Rudomin and Schmidt 1999; Betley et al. 2009). In the vertebrate spinal cord the phenomenon was characterised as primary afferent depolarisation, and the axo-axonic synapse was identified as its substrate (Rudomin and Schmidt 1999); it supplied the cellular mechanism on which the gate control theory of pain was built (Melzack and Wall 1965; Mendell 2014).

What is known about its organisation has been assembled one modality at a time, and largely in different animals. In *Drosophila*, GABAergic local interneurons of the antennal lobe inhibit olfactory receptor neuron terminals through gamma-aminobutyric acid type B (GABA-B) receptors, with a receptor density that varies between glomeruli and a measurable consequence for mate localisation (Root et al. 2008); the same interneurons implement a gain control whose strength scales with the total feedforward drive reaching the antennal lobe, so that the inhibition is set by global rather than glomerulus-specific activity (Olsen and Wilson 2008). In mouse spinal cord, a molecularly defined population of GABApre interneurons contacts proprioceptive afferent terminals with a sensory-to-motor preference of approximately 2,000 to 1, and fails to form synapses at all when that target is removed (Betley et al. 2009); genetic ablation of these interneurons leaves goal-directed reaching oscillatory, which establishes that the axo-axonic contact is required for normal behaviour (Fink et al.

2014). In rat lamina I, presynaptic inhibition of C-fibre input is recruited by the C-fibres themselves, a homotypic feedforward arrangement that regulates how much nociceptive afferent activity is required to excite projection neurons (Fernandes et al. 2020), and parvalbumin-expressing dorsal horn interneurons have been identified as a likely source of axo-axonic input onto myelinated afferent terminals (Hughes et al. 2012).

Each of these is a detailed account of one circuit, but neither individually nor together do they answer two questions that only a complete inventory can address. First, is presynaptic inhibitory control partitioned by modality, with dedicated inhibitors for each afferent class, or do shared interneuron pools serve several classes? Betley et al. (2009) reported that proprioceptive and cutaneous afferents appeared to be contacted by distinct subsets of a common transcriptional lineage and proposed diversification by modality, but could not enumerate the subsets. The inhibitory interneurons of the mammalian dorsal horn are themselves still being resolved into functional populations, and the assignment of particular populations to particular afferent classes remains incomplete (Todd 2017). Second, and with more direct clinical bearing, is the control of some modalities architecturally more fragile than that of others? That question has not been addressed quantitatively, because answering it requires counting every inhibitory synapse onto every afferent of every class within one nervous system, a measurement that no mammalian preparation supports.

The clinical motivation is specific. Loss of spinal GABAergic inhibition is a central mechanism of neuropathic pain: partial peripheral nerve injury selectively reduces GABAergic transmission in the superficial dorsal horn (Moore et al. 2002), and a trans-synaptic collapse of the transmembrane chloride gradient in lamina I neurons converts anionic inhibition into excitation (Coull et al. 2003). In *Drosophila*, peripheral nerve injury kills GABAergic neurons in the ventral nerve cord (VNC) and produces thermal and mechanical hypersensitivity (Khuong et al. 2019). Disinhibition of this kind reliably produces pain rather

than a proprioceptive or tactile deficit of comparable severity, and the spinal microcircuit through which low-threshold mechanical input gains access to nociceptive output once inhibition is lifted has been resolved genetically in mouse (Duan et al. 2014). Whether that asymmetry has a structural basis, that is, whether nociceptive afferents simply have less redundant inhibitory control to lose, has remained a matter of inference.

Drosophila melanogaster is an unexpected preparation for a question framed around pain, and the grounds for it should be stated. The fly has dedicated nociceptors. The class IV multidendritic neurons of the larval body wall require the *painless* transient receptor potential channel to respond to noxious heat and harsh touch (Tracey et al. 2003), and their activation alone is sufficient to trigger the stereotyped rolling escape that larvae use against parasitoid wasps (Hwang et al. 2007); the molecular and behavioural repertoire of larval nociception has since been characterised in detail (Im and Galko 2012). In the adult, the abdominal multidendritic afferents, which are larval class IV neurons that survive metamorphosis, are the only somatosensory class whose activation produces both rapid escape and sustained place avoidance, and they form their strongest connections with ascending interneurons projecting to the brain (Jones et al. 2025); these are the afferents and ascending neurons analysed here. The central processing of this input is itself shaped by inhibition: mechanosensory and nociceptive cues converge at several levels to enhance escape selection (Ohyama et al. 2015), reciprocally connected inhibitory interneurons implement behavioural choice by disinhibition (Jovanic et al. 2016), serotonergic feedback sensitises nociceptor terminals to presynaptic inhibition in a pathway-specific manner (Kaneko et al. 2017), and dedicated interneurons couple nociceptive input to modular motor output (Burgos et al. 2018). Nociception in this animal is therefore neither incidental nor poorly characterised, which is what makes a structural census of its inhibitory control interpretable.

Volumetric electron microscopy (EM) connectomes now make that census possible. Synapse-resolution wiring diagrams were for three decades available for *Caenorhabditis elegans* alone (White et al. 1986; Varshney et al. 2011); since 2020 they have been produced for the *Drosophila* central brain (Scheffer et al. 2020), for the larval brain (Winding et al. 2023), and for the whole adult female brain together with its cell-type annotation and network statistics (Dorkenwald et al. 2024; Lin et al. 2024; Schlegel et al. 2024). Three independently acquired datasets, spanning two males and one female, were used here to census the complete inhibitory input onto every class of sensory afferent. The study aimed to determine whether that control is partitioned by modality, whether any partition is enforced synaptically rather than by spatial segregation, whether the control of nociceptive afferents differs in concentration from that of the other sensory modalities, and how that control is organised across the body.

Materials and methods

Datasets

Three publicly released adult *D. melanogaster* EM connectomes were analysed. The male-CNS v1.0 dataset (Janelia Research Campus) comprises the complete central nervous system (CNS) of one male (Berg et al. 2026). The released annotation table contains 211,577 bodies, of which 166,700 carry a superclass assignment and 164,506 a cell-type assignment; the connectivity analysed here comprises 25,563,197 neuron-to-neuron connections and 124,025,046 synapses. The Male Adult Nerve Cord (MANC) dataset, version 1.2.1, comprises the VNC of a second male (23,650 neurons; 5,305,354 connections) (Takemura et al. 2024), systematically annotated by cell type and developmental hemilineage (Marin et al. 2024) and analysed previously for the organisation of its descending-to-motor pathways (Cheong et al. 2026). The Brain And Nerve Cord (BANC) dataset, release 888, comprises the brain and VNC of a female (188,508 neurons; 13,620,865 connections) (Bates et al. 2026).

MANC and BANC were obtained in a harmonised metadata format (see Data availability). No connection-weight threshold was applied to any reported proportion unless stated.

Definition of afferent classes

Afferent classes were defined from the native annotation of each dataset. In male-CNS, sensory neurons were those whose superclass contained the term sensory, and classes were taken from the class and subclass fields: olfactory, thermosensory, hygrosensory, gustatory, visual, tactile, cephalic mechanosensory, and the chordotonal, campaniform and hair-plate subclasses of proprioceptive neurons, which correspond to the functionally characterised mechanosensory and proprioceptive organs of the insect body (Tuthill and Wilson 2016; Mamiya et al. 2018). Nociceptive multidendritic (md) afferents were defined as cell types SNch01 (abdominal), SNxx29, SAxx02 and SNxx25 (leg and wing), following the published definition of adult multidendritic nociceptors (Jones et al. 2025), and were removed from any other class to which the annotation would otherwise assign them. In MANC and BANC, the corresponding native cell-class fields were used; in BANC the annotated multidendritic neuron class was used in preference to cross-dataset type matching, which proved unreliable for this class (see Discussion).

Census and concentration indices

For each afferent class, all incoming connections were summed to give total synaptic input, including synapses made onto the afferents by other sensory afferents. The GABAergic fraction was identified from the neurotransmitter prediction supplied with each dataset, which is derived from synaptic ultrastructure by a convolutional classifier reported to be 94% accurate at the level of the individual neuron (Eckstein et al. 2024), and was decomposed by presynaptic cell type. Two concentration indices were computed over the shares of GABAergic input by source cell type: N50, the smallest number of source cell types whose shares sum to at least 50%, and the Herfindahl-Hirschman index (HHI), the sum of the

squared shares. A low N50 and a high HHI indicate control concentrated in few sources. For AN05B004, input from and output to the nociceptive afferents were further resolved by the afferent body region (abdominal, or leg and wing) and by side, taken from the root-side annotation of each afferent.

Hemilineage analysis

Hemilineages are the developmental units of the insect nerve cord, within which fast-transmitter identity is uniformly specified at the level of the neuroblast (Lacin et al. 2019). For each of the 116 GABAergic cell types of hemilineage 05B with more than 500 output synapses (of 117 in total), the fraction of total output reaching each afferent class was computed. The reciprocal analysis identified, for each afferent class, the GABAergic cell type supplying the largest share of its input.

Null model for reciprocal wiring

A reciprocity statistic was defined for each neuron as the fraction of its total output synapses landing on sensory neurons that also synapse onto it, using a minimum weight of three synapses to define a connection. The statistic was computed for all ascending neurons and, separately, for all 9,767 GABAergic neurons with more than 500 output synapses. The null distribution was generated by degree-preserving edge swapping (Maslov and Sneppen 2002) on the 59,536 connections that run from these GABAergic neurons onto sensory neurons, which involve 1,633 of them. Postsynaptic targets were exchanged between connections while each presynaptic neuron retained its own weights, preserving every out-degree and in-degree. Five hundred randomisations were performed, each with twice as many swaps as connections, and z scores and empirical p values were computed against the resulting distribution.

Test of positional against synaptic specificity

Centreline skeletons in SWC format were obtained for the neurons of interest and for 14 afferents of each of three classes, and were converted from 8 nm voxel units to micrometres.

Each neuron's arbor was represented as the set of 5 μm voxels occupied by its nodes. For each 05B neuron, the proportion of the nodes of each afferent class falling inside that voxel set was computed and compared with the proportion of the neuron's output synapses reaching that class. Co-location without connection indicates specificity that spatial segregation does not explain.

Synapse localisation

Synapse-level coordinates were taken from the male-CNS v1.0 synaptic partner table (124,039,080 records), read in batches and filtered to the connections of interest. Postsynaptic coordinates were converted from 8 nm voxel units to micrometres. For every synapse made by nociceptive afferents onto the ascending projection neurons, the Euclidean distance to the nearest synapse made by AN05B004 onto the afferents was computed with a k-dimensional tree. A null expectation was generated by redistributing the inhibitory synapses uniformly at random within the bounding volume they occupy and recomputing the same distances. The same procedure was applied to the reciprocal pair of synapse populations.

Network simulation

A leaky integrate-and-fire (LIF) network was built directly on the measured connectivity, with the parameters published for the whole-brain *Drosophila* model (Shiu et al. 2024): resting and reset potential −52 mV, threshold −45 mV, membrane time constant 20 ms, synaptic time constant 5 ms, refractory period 2.2 ms, synaptic delay 1.8 ms and 0.275 mV per synapse. Cholinergic connections were excitatory, and GABAergic and glutamatergic connections were inhibitory, following the same model, because glutamate acts largely through inhibitory chloride channels in the insect CNS. The principal model comprised the VNC together with ascending and descending neurons (24,154 neurons; 4,036,154 connections), the structure analogous to the spinal cord. Recurrent connections between Kenyon cells were excluded from whole-CNS runs because they produce non-physiological runaway activity in this model

class. Sensory neurons were driven as Poisson processes at defined rates, and silencing was implemented by setting a neuron's output to zero. Each condition was run for 1 s of simulated time with two to eight trials. Robustness was assessed across synaptic weights from 0.10 to 0.275 mV, with glutamate treated as excitatory, with neurons of uncertain neurotransmitter made neutral, and with connections restricted to those of at least five synapses.

Control analyses

Four controls were performed. First, the effect of silencing was decomposed by removing selectively the synapses of AN05B004 onto afferent terminals, onto the ascending pathway, and onto all other targets. Second, presynaptic inhibition was implemented in its mechanistically appropriate form, by multiplying the output weights of nociceptive afferents by a release factor s, because a point-neuron model cannot otherwise represent axo-axonic inhibition. Third, a network-instability control removed 5,318 cholinergic neurons, matching the number of VNC GABAergic neurons, and recorded global mean firing rate alongside pathway output. Fourth, a null distribution of the silencing effect was generated by silencing, one at a time, each of the 71 GABAergic cell types making at least 10 synapses onto the nociceptive pathway.

Computational analysis and use of artificial intelligence

Large language models were used to implement the analyses for three reasons. First, the study is a complete census rather than a sample: it covers every afferent class in three connectomes comprising more than 44 million neuron-to-neuron connections, and its conclusions depend on a large number of supporting analyses, including 500 degree-preserving randomisations, the silencing of each of 71 GABAergic cell types, screens of 252 cell types and simulations across model variants and datasets. The work was carried out without funding, and implementation by language models made it feasible to analyse the full census, rather than a subset of afferent classes, while keeping every step in executable code. Second, the use of

language models made possible a verification design that is rarely available to a single analyst: an independent reimplementation written from the Methods alone, which tests whether the written methods are sufficient to reproduce the results, and an adversarial review whose explicit aim was to refute the interpretation. Third, the analyses are computations on public data, so their correctness can be judged directly from the released code and its output, independently of how the code was written. The known risk of language-model output, namely silent errors in code, was addressed by the controls described below, and the scientific decisions were made by the authors: the research question, the definition of afferent classes, the indices of concentration, the choice of positive control, the control analyses to be retained and the interpretation of the results.

All analyses reported in this study were implemented and executed by large language models operating in an agentic coding environment, in Python 3 with pandas, NumPy, SciPy and Numba, with figures drawn in matplotlib, in November 2026. This includes the construction of the census tables and concentration indices, the degree-preserving null model, the skeleton-based test of co-location, the synapse-localisation analysis, the LIF simulations, every control analysis and every figure. The primary analysis was performed by Claude Opus models (Anthropic; model identifiers claude-opus-5 and claude-opus-5-5, both of which served the working session). The complete structural analysis was then reimplemented from the written methods alone, without access to the original code, by a separate model (Claude Fable, Anthropic). The reciprocity statistic agreed to four decimal places, and two discrepancies were identified and corrected in the primary analysis: an undeclared minimum-synapse threshold and an afferent definition applied inconsistently across datasets. The interpretation was then subjected to adversarial review by a third model (Claude Sonnet, Anthropic) instructed to refute it; three objections were upheld and generated the decomposition, instability and null-distribution controls reported here. The complete pipeline, from data

retrieval and the definition of afferent classes to the null model, the synapse-localisation analysis, the LIF simulations and the control analyses, was then reproduced step by step by a computer engineer among the authors (R.M.R.), who rebuilt each analysis with the public data and tools, with the assistance of a language model, and confirmed the reported results. A one-page preliminary document prepared with these models to assess the feasibility of the study was entirely rewritten by the authors. Every number reported in the text was checked by the authors against the output table that produced it. The research question, the scope of the census and the verification strategy were defined by the authors, as detailed under Author contributions, and all authors take full responsibility for the analyses, their interpretation and the final text. Verification of the computational work therefore rests on five independent elements: the reimplementation from the written methods, which detected and led to the correction of two errors; the step-by-step reproduction of the complete pipeline by a computer engineer; the recovery from anatomy alone of an experimentally established positive control, presynaptic inhibition in the antennal lobe; the replication of the main result in three independently acquired connectomes; and the release of the complete analysis code and derived tables (Online Resources 2 and 3), so that every result can be re-executed. This use of artificial intelligence is reported in accordance with the journal's policy, and no model is listed as an author.

Results

Inhibitory control of sensory afferents is partitioned by modality

Eleven afferent classes were identified in male-CNS (Table 1). Visual afferents received 2.5% of their input from GABAergic sources and were not considered further. The three classes that terminate in the antennal lobe, olfactory, thermosensory and hygrosensory, shared a single dominant inhibitor, the lLN2F_b local interneurons. Each of the remaining seven classes was dominated by a different GABAergic cell type, and none of these seven cell types was the

largest source for any other class (Figs. 1a, 2). The GABAergic share of total input ranged from 28% for olfactory afferents to 84% for hair-plate proprioceptors, and the largest single source ranged from 3% to 57% of total input.

The method recovered a known case as a positive control. Olfactory afferents had N50 = 1, with lLN2F_b supplying 14.5% of their total input (Fig. 2c). Presynaptic inhibition of olfactory receptor neuron terminals by GABAergic local interneurons of the antennal lobe, acting through GABA-B receptors with glomerulus-specific strength and a measurable effect on mate localisation, is established experimentally (Olsen and Wilson 2008; Root et al. 2008). The same result was obtained independently in BANC (lLN2F_b, 23.0% of olfactory input), where thermosensory and hygrosensory afferents were likewise dominated by this cell type.

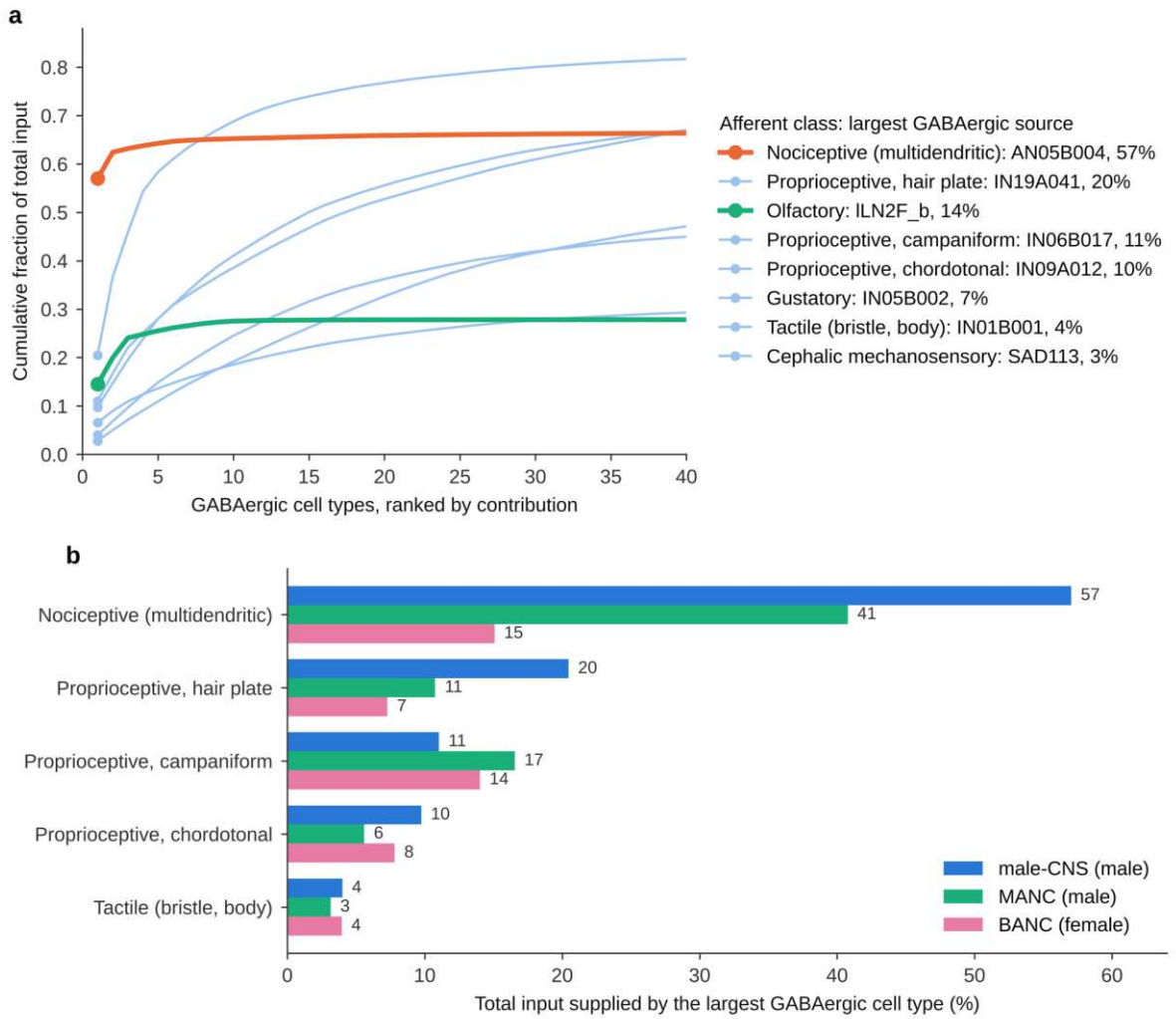


Fig. 1 Concentration of inhibitory control by afferent class. **a** Cumulative share of total synaptic input supplied by GABAergic cell types, ranked from largest to smallest, one curve per afferent class (male-CNS v1.0). Each class is labelled with its largest GABAergic source and the share of total input that source supplies. The nociceptive curve reaches 57% at its first cell type. The olfactory curve, shown as a positive control, reproduces an experimentally established case; thermosensory and hygrosensory afferents share its dominant source and are omitted for clarity. **b** Share of total afferent input supplied by the single largest GABAergic cell type for the five somatosensory classes present in all three connectomes

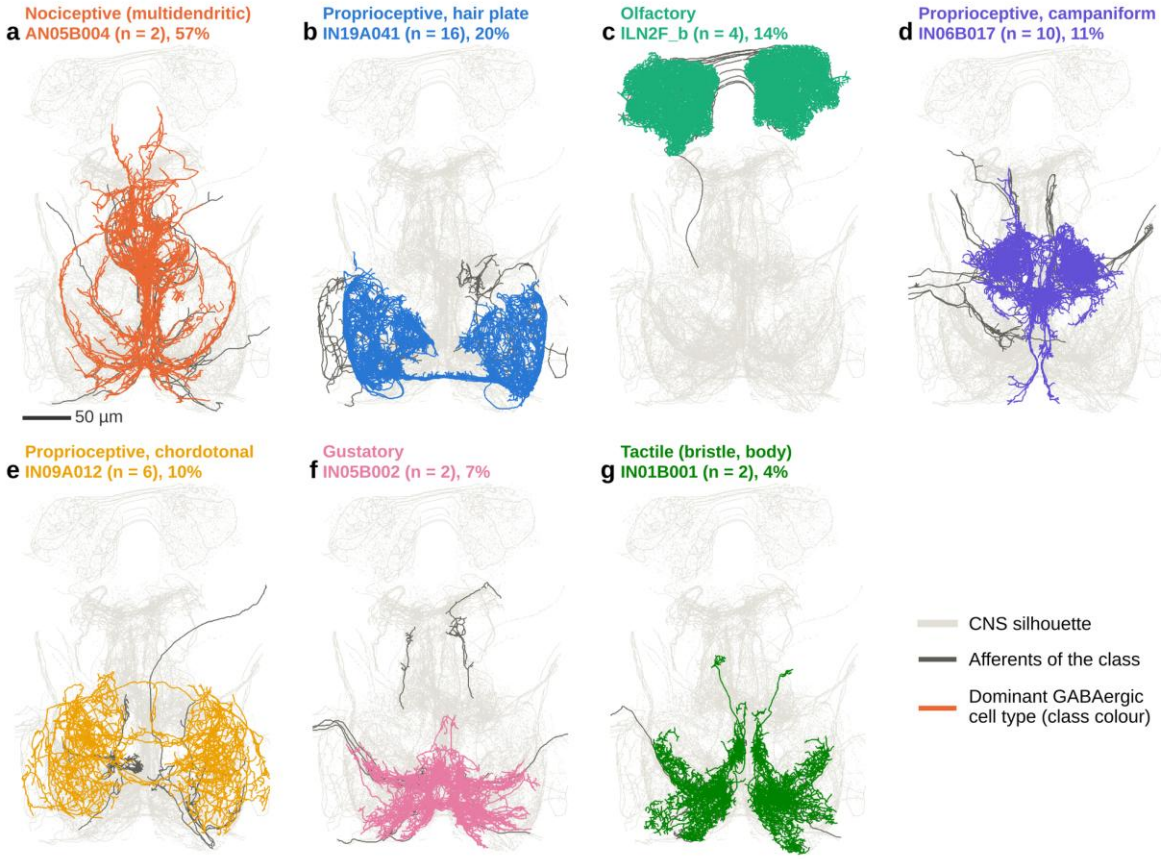


Fig. 2 The census rendered anatomically. Each panel shows one afferent class (dark grey) with its dominant GABAergic cell type (colour), over a silhouette of the central nervous system assembled from all neurons in the figure (light grey). The label gives the dominant cell type, the number of neurons of that type (*n*) and its share of the total synaptic input of the class. **a** Nociceptive (multidendritic). **b** Proprioceptive, hair plate. **c** Olfactory. **d** Proprioceptive, campaniform. **e** Proprioceptive, chordotonal. **f** Gustatory. **g** Tactile (bristle, body). All panels share scale and framing; frontal view, male-CNS v1.0. Scale bar 50 µm

Nociceptive afferents are the most concentrated somatosensory class

Nociceptive md afferents had the most concentrated inhibitory control of any somatosensory class in all three datasets, and of any class at all in the complete male CNS. In male-CNS, a single bilateral pair of GABAergic ascending neurons, AN05B004, supplied 57.0% of all synaptic input onto the 77 nociceptive afferents (N50 = 1; HHI 0.733), against 20.5% for the largest source onto hair-plate proprioceptors, 11.0% for campaniform proprioceptors, 9.7% for chordotonal proprioceptors, 6.5% for gustatory afferents, 4.0% for tactile afferents and

2.8% for cephalic mechanosensory afferents (Table 1; Figs. 1a, 2a). AN05B004 made no measurable contribution (0.0%) to the input of any other afferent class.

Among classes with substantial inhibitory control, defined as more than half of total input being GABAergic, the nociceptive class was the only one with N50 = 1. Olfactory, thermosensory and hygrosensory afferents also showed a low N50 but received less than 40% of their input from GABAergic sources, so the absolute magnitude of the concentrated control was smaller. The ordering was preserved across animals: the largest single GABAergic source supplied 57.0% of nociceptive afferent input in male-CNS, 40.8% in MANC and 15.1% in BANC, in each case the highest value among the somatosensory classes of that dataset (Fig. 1b). In BANC the antennal-lobe classes reached higher values (23.0% for olfactory and 23.2% for thermosensory afferents), but less than 40% of their input was GABAergic (Online Resource 1, Table S1). The circuit connectivity is summarised for the three connectomes in Online Resource 1, Fig. S1.

The concentration was not an artefact of a small denominator. Nociceptive afferents received 24,706 input synapses in total, approximately 321 per neuron, which is more per neuron than chordotonal proprioceptors received (109).

Table 1 Census of inhibitory input by afferent class, male-CNS v1.0

Afferent class	Afferents (n)	Input synapses	GABA (%)	GABA cell types (n)	Largest GABA source	Share of input (%)	N50	HHI
Nociceptive (multidendritic)	77	24,706	66.9	121	AN05B004	57.0	1	0.733
Proprioceptive, hair plate	113	11,218	83.8	144	IN19A041	20.5	3	0.126
Thermosensory	25	12,862	23.4	18	lLN2F_b	16.8	1	0.538
Olfactory	2,639	431,288	27.8	56	lLN2F_b	14.5	1	0.334
Hygrosensory	66	17,231	26.5	26	lLN2F_b	12.7	2	0.325
Proprioceptive, campaniform	426	90,205	79.9	497	IN06B017	11.0	11	0.040
Proprioceptive, chordotonal	425	46,314	77.8	332	IN09A012	9.7	9	0.040
Gustatory	1,428	283,851	31.4	243	IN05B002	6.5	7	0.067
Tactile (bristle, body)	2,558	350,517	50.2	364	IN01B001	4.0	11	0.033
Cephalic mechanosensory	1,733	132,841	63.9	364	SAD113	2.8	20	0.018
Visual	6,091	215,825	2.5	18	C2	2.1	1	0.720

Classes are ordered by the share of total input supplied by the largest GABAergic source. *GABA (%)*, share of total input from GABAergic neurons; *N50*, smallest number of GABAergic cell types supplying at least half of the GABAergic input of the class; *HHI*, Herfindahl-Hirschman index of the GABAergic input shares

Sibling cell types of one hemilineage target different afferent classes

Of the 116 GABAergic cell types of hemilineage 05B analysed, AN05B004 directed 52.6% of its output to nociceptive afferents, against 0.9% for the next-ranked sibling, a difference of approximately 58-fold (Fig. 3; Online Resource 1, Table S2). Other siblings were also axo-axonic but targeted different classes: AN05B023a directed 61.6% of its output to gustatory afferents, IN05B019 directed 66.6% to tactile bristle afferents, and IN05B016 directed 33.1% to campaniform proprioceptors. No 05B cell type directed a substantial share of its output to hair-plate proprioceptors, whose dominant inhibitor, IN19A041, belongs to a different hemilineage. The hemilineage therefore behaves as a family of modality-dedicated inhibitors rather than as a generic pool, although the dominant inhibitors of the different afferent classes are drawn from several hemilineages (Fig. 2).

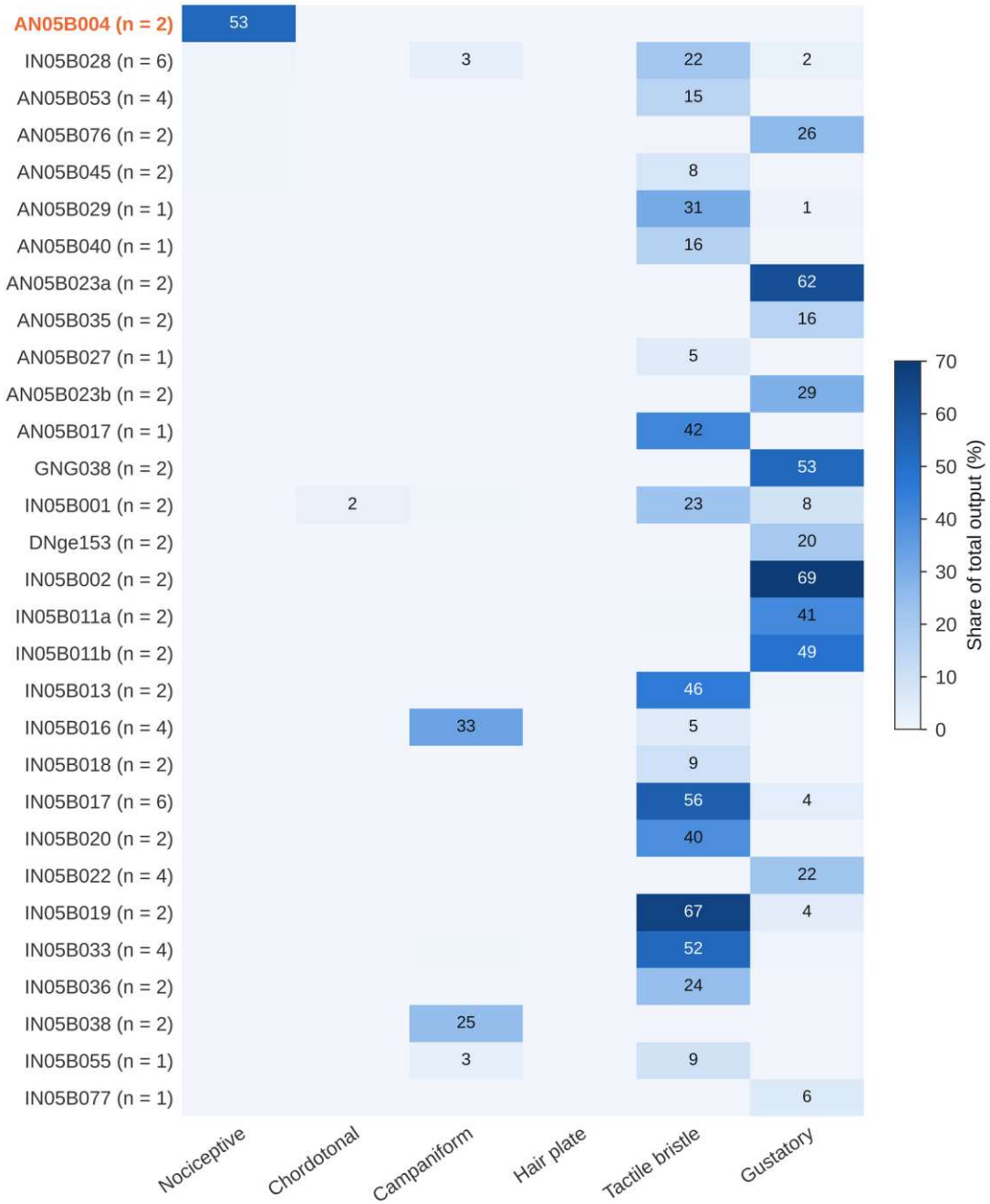


Fig. 3 Hemilineage 05B as a family of modality-dedicated inhibitors. Share of the total output of each GABAergic 05B cell type that reaches each afferent class, in percent (male-CNS v1.0). Only cell types directing at least 5% of their output to one class are shown; *n* is the number of neurons of each type, and AN05B004 is highlighted. Chordotonal, campaniform and hair-plate afferents are proprioceptive; tactile bristle afferents are those of the leg and notum

Specificity is synaptic, not positional

To test whether this partition reflects spatial segregation, the arbors of three 05B neurons were reconstructed from their skeletons, and the proportion of each afferent class lying inside each arbor was compared with the proportion of output actually reaching that class (Table 2; Fig. 4). AN05B023a contained 42.1% of the nodes of nociceptive afferents within its own arbor, a higher proportion than it contained of its own target class (14.0% for gustatory afferents), yet directed 0.1% of its output to nociceptors and 61.6% to gustatory afferents. AN05B004 contained 11.9% of gustatory and 9.6% of tactile afferent nodes but directed 0.1% and 0.0% of its output to them. IN05B019 contained 12.5% of nociceptive afferent nodes and directed 0.0% of its output to them. Co-location therefore does not predict connection, and the partition is enforced at the synapse.

Table 2 Spatial co-location against synaptic connection for three GABAergic cell types of hemilineage 05B

Neuron	Afferent class	Afferent nodes inside arbor (%)	Output reaching the class (%)
AN05B004	Nociceptive (target)	56.9	52.6
AN05B004	Gustatory	11.9	0.1
AN05B004	Tactile	9.6	0.0
AN05B023a	Nociceptive	42.1	0.1
AN05B023a	Gustatory (target)	14.0	61.6
AN05B023a	Tactile	0.5	0.0
IN05B019	Nociceptive	12.5	0.0
IN05B019	Gustatory	0.1	3.9
IN05B019	Tactile (target)	47.9	66.6

Male-CNS v1.0; 14 afferents per class. Arbors were represented as the set of 5 µm voxels occupied by their skeleton nodes

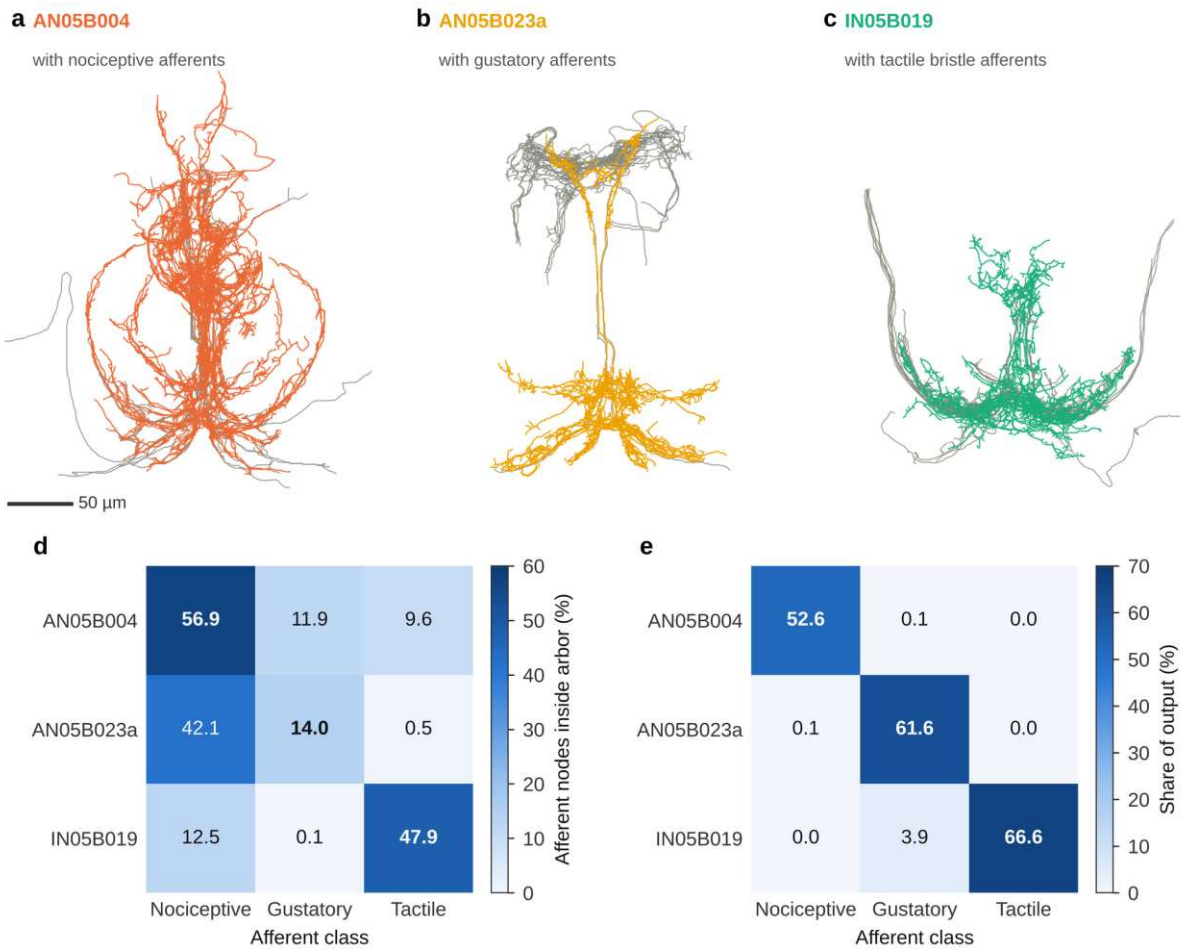


Fig. 4 Specificity is synaptic, not positional. **a**, **b**, **c** Three GABAergic 05B neurons (colour) shown with the afferent class each innervates (grey), frontal view, male-CNS v1.0: AN05B004 with nociceptive afferents (**a**), AN05B023a with gustatory afferents (**b**) and IN05B019 with tactile bristle afferents (**c**). Scale bar 50 µm. **d** Percentage of the skeleton nodes of each afferent class that lie inside the arbor of each neuron. **e** Percentage of the output synapses of each neuron that reach each class. Values in bold correspond to the target class of each neuron

Inhibitory synapses are placed on the release sites

Synapse-level coordinates reproduced the connection counts obtained independently from the connectivity table: 14,090 synapses from AN05B004 onto nociceptive afferents, 15,385 in the reverse direction and 32,680 from nociceptive afferents onto the ascending projection neurons (Fig. 5a, b). The inhibitory synapses were not distributed diffusely along the afferent arbor. For every synapse made by a nociceptive afferent onto the ascending pathway, the nearest

AN05B004 synapse lay at a median distance of 1.30 µm (interquartile range 0.86 to 2.18 µm). Redistributing the same inhibitory synapses uniformly within the volume they occupy gave a median of 7.32 µm, so the observed arrangement was 5.6-fold closer than chance (Fig. 5c). The reciprocal synapses were closer still: the median distance between a synapse from a nociceptor onto AN05B004 and the nearest synapse from AN05B004 onto a nociceptor was 0.95 µm, indicating that the loop closes locally rather than across the neuropil. This is the spatial arrangement that axo-axonic presynaptic inhibition requires, and it was measured directly rather than inferred from the simulation.

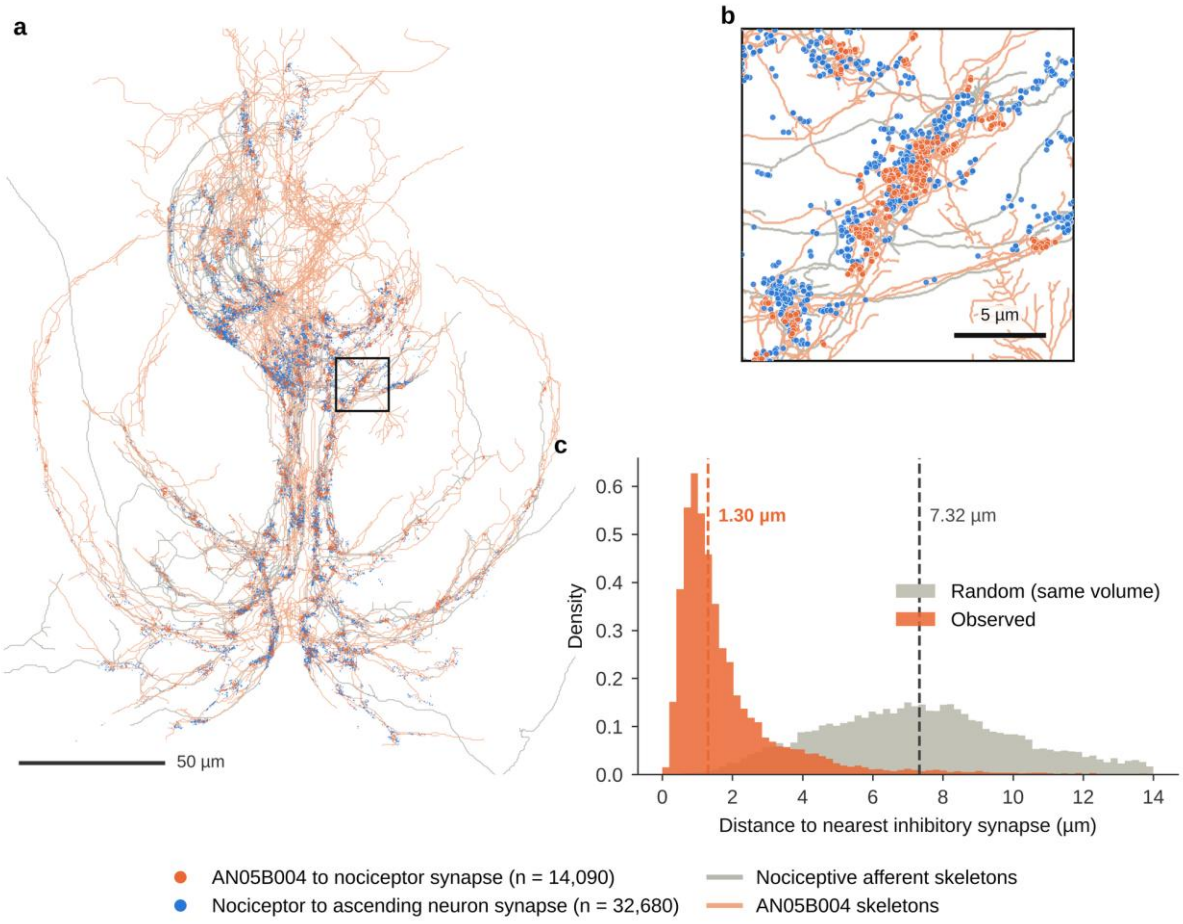


Fig. 5 Inhibitory synapses are placed on the afferent release sites. **a** All 46,770 synapses of the circuit at their measured coordinates, over the reconstructed skeletons of the nociceptive afferents and of AN05B004, frontal view, male-CNS v1.0. The box marks the densest region, enlarged in **b**. Scale bar 50 µm. **b** Enlargement of the boxed region, drawn from high-resolution skeletons. Scale bar 5 µm. **c** Distance from each afferent output synapse (nociceptor onto ascending neuron) to the nearest inhibitory synapse (AN05B004 onto

nociceptor), observed, against the distribution expected when the same inhibitory synapses are redistributed at random within the volume they occupy. Dashed lines mark the medians

Reciprocal wiring exceeds chance but is common

AN05B004 formed a closed loop with nociceptive afferents, receiving 54.8% of its own input from them and returning 52.6% of its output to their terminals (Fig. 6). Under the degree-preserving null model, the expected reciprocity for the two AN05B004 neurons was 0.013 (standard deviation 0.011), against observed values of 0.812 and 0.799, corresponding to z = 74.8 and z = 80.4 ($p < 0.002$); no randomisation of 500 reached the observed value, and the highest value attained by any neuron in any randomisation was 0.195 (Fig. 7a).

Reciprocal axo-axonic wiring was not, however, unique to AN05B004. Among all 9,767 GABAergic neurons with more than 500 output synapses, the two AN05B004 neurons ranked 16th and 21st, behind IN19A041 (0.932) and IN01B001 (0.882), the dominant inhibitors of hair-plate and tactile afferents respectively (Fig. 7b). The motif is therefore common in the VNC; what distinguishes the nociceptive class is the concentration of that motif in a single source, not the motif itself.

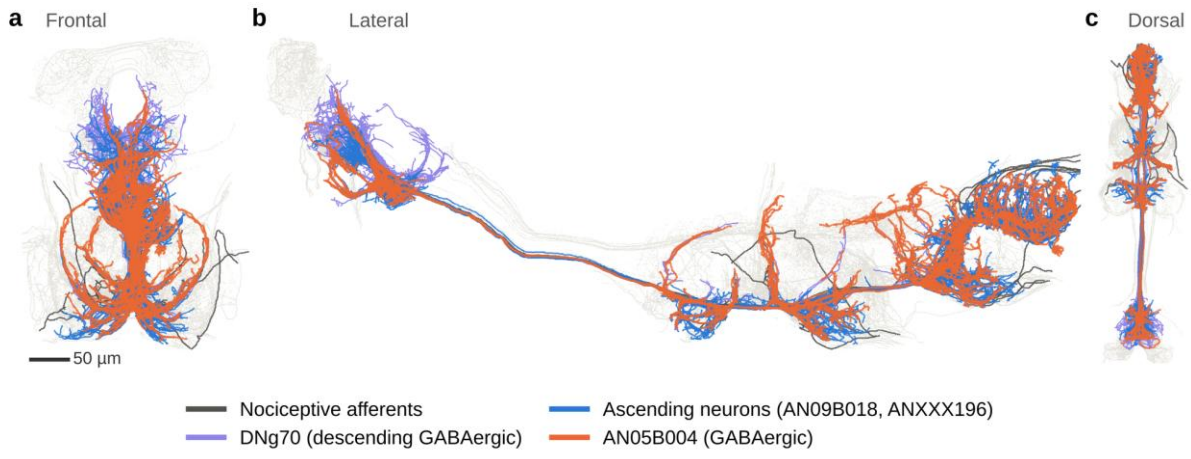


Fig. 6 The nociceptive loop in three views. Nociceptive afferents, AN05B004, the ascending projection neurons AN09B018 and ANXXX196, and the descending neuron DNg70, reconstructed from skeletons over the silhouette of the central nervous system (light grey), male-CNS v1.0. **a** Frontal view. **b** Lateral view. **c** Dorsal view. Scale bar 50 µm, applies to all panels

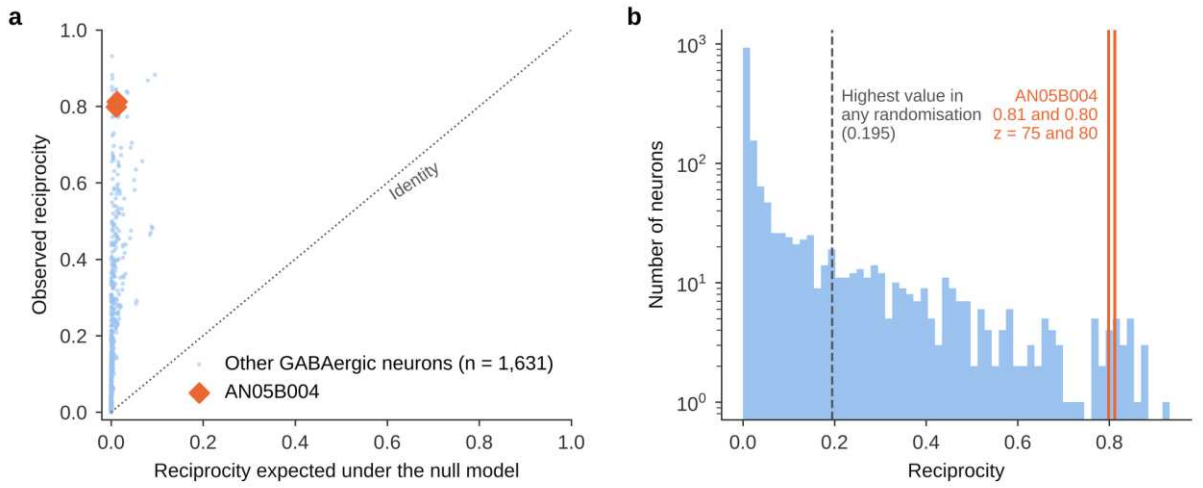


Fig. 7 Reciprocal wiring against a degree-preserving null model. Reciprocity is the fraction of the output of a neuron that returns to the sensory neurons from which it receives input. **a** Observed reciprocity against the value expected under 500 degree-preserving randomisations, for the 1,633 GABAergic neurons (of 9,767 with more than 500 output synapses) that contact sensory afferents. The dotted line marks identity. **b** Distribution of observed values, with a logarithmic vertical axis. The dashed line marks the highest value attained by any neuron in any randomisation, and the two solid lines mark the two AN05B004 neurons

One inhibitor pools nociceptive input from the whole body

The loop was not organised segment by segment. Each of the two AN05B004 neurons received synapses from all 77 nociceptive afferents and made synapses onto all 77, spanning the abdomen, legs and wings on both sides of the body (Fig. 6). Input to each neuron was divided almost equally between afferents of the left and right sides (4,163 and 3,540 synapses for one neuron; 3,873 and 3,809 for the other) and between abdominal and leg or wing afferents (approximately 3,000 and 4,700 synapses for each neuron), and output was distributed in similar proportions. The arrangement was reproduced in MANC, where each AN05B004 neuron received input from all 82 nociceptive afferents and contacted 81 or 82 of them. AN05B004 therefore pools nociceptive drive from the whole body and returns inhibition to every nociceptive terminal.

The nociceptive afferents were also coupled to each other: synapses between nociceptive afferents supplied 23.6% of their total input in male-CNS and 34.1% in MANC. Because

these synapses are cholinergic, the abdominal afferents of MANC receive slightly more cholinergic than GABAergic input (53.6% against 45.1%), most of it (42.0% of the total) from other abdominal afferents, in agreement with the report that adult md neurons receive predominantly cholinergic input (Jones et al. 2025). Among sources other than the afferents themselves, AN05B004 was the largest in both datasets, supplying 55.1% of the total input onto abdominal afferents in male-CNS and 37.2% in MANC. A second GABAergic source, the descending neuron DNg70, supplied 10.1% of the input onto the leg and wing nociceptive afferents in male-CNS (Online Resource 1, Fig. S1).

Functional consequence in simulation

In the LIF model, driving abdominal nociceptive afferents at 20 Hz produced a mean firing rate of 30.0 Hz in the ascending nociceptive projection neurons AN09B018 and ANXXX196. Silencing AN05B004 raised this to 108.3 Hz, a 3.6-fold increase, while global mean network activity fell slightly, from 6.8 to 6.0 Hz (Table 3; Fig. 8a). The stimulus-response threshold, defined as the afferent firing rate required to drive the ascending pathway to 20 Hz, fell from 15.3 to 5.5 Hz (Online Resource 1, Fig. S2a).

The effect ranked first among the 71 GABAergic cell types making at least 10 synapses onto the pathway (fold change 3.57; median 1.02; 95th percentile 1.02), and the second-ranked type was the descending neuron DNg70 (1.60) (Fig. 8b; Online Resource 1, Table S3). Normalised per synapse, AN05B004 ranked 53rd of 71, indicating that its influence derives from the volume of its connection, 15,264 synapses onto the pathway against 2,060 for the next-ranked type, rather than from greater efficacy per synapse.

The direction of the effect was preserved across all model variants: 1.8- to 3.5-fold for abdominal afferent drive and 2.2- to 6.0-fold for leg afferent drive across synaptic weights of 0.10 to 0.275 mV, 3.9- and 8.5-fold with glutamate treated as excitatory, 2.9- and 3.4-fold with uncertain neurotransmitters made neutral, and 3.4- and 5.4-fold with connections

restricted to at least five synapses (Online Resource 1, Fig. S3, Table S4). In the independent MANC connectome the effect was 2.1- to 4.6-fold, and in BANC, where only the leg afferent pathway was adequately reconstructed, it was 1.5- to 1.8-fold (Online Resource 1, Fig. S4c).

Table 3 Pathway-specific against global effects in the network model

Condition	Afferent drive	Ascending output (Hz)	Global mean activity (Hz)	Ratio
Intact	Nociceptive, 20 Hz	30.0	6.8	4.4
AN05B004 silenced (2 neurons)	Nociceptive, 20 Hz	108.3	6.0	17.9
DNg70 silenced (2 neurons)	Nociceptive, 20 Hz	47.9	7.3	6.5
AN05B004 and DNg70 silenced	Nociceptive, 20 Hz	200.0	8.2	24.4
All 5,318 VNC GABAergic neurons removed	Nociceptive, 20 Hz	54.8	57.2	1.0
Intact	Tactile, 50 Hz	0.0	11.7	n/a
All 5,318 VNC GABAergic neurons removed	Tactile, 50 Hz	50.2	76.4	0.7
5,318 cholinergic neurons removed (3 draws)	Tactile, 50 Hz	0.0	7.5 to 7.7	n/a
5,318 random inhibitory neurons removed	Tactile, 50 Hz	94.6	95.4	1.0

Ascending output is the mean firing rate of the projection neurons AN09B018 and ANXXX196; the ratio is ascending output divided by global mean activity. *VNC*, ventral nerve cord; *n/a*, not applicable because ascending output was zero

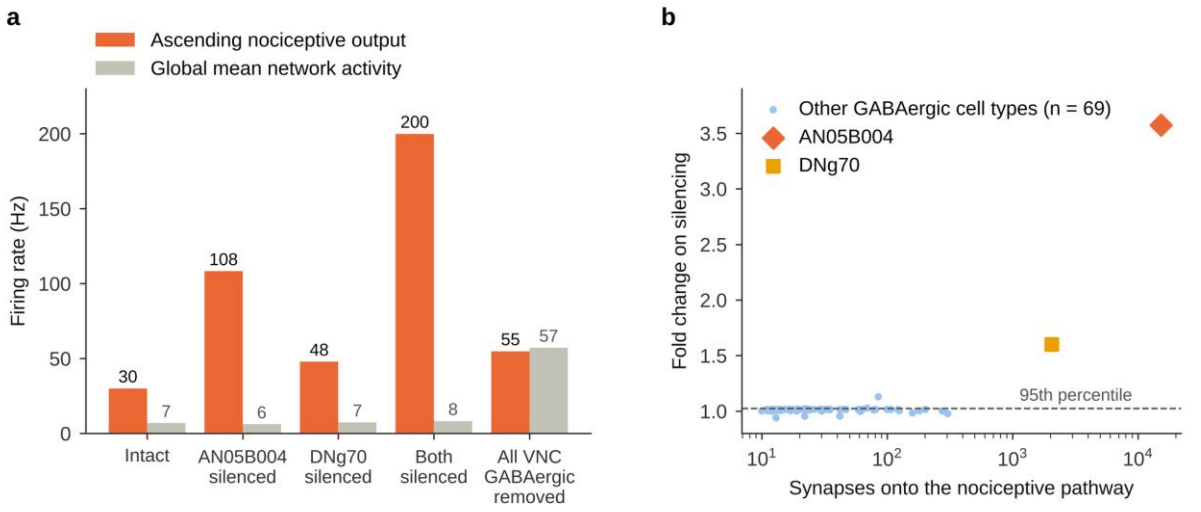


Fig. 8 Specific disinhibition against network collapse in the network model. **a** Ascending nociceptive output and global mean network activity under 20 Hz drive of abdominal nociceptive afferents, with the network intact, with AN05B004 or DNg70 silenced (two neurons each), with both silenced, and with all 5,318 GABAergic neurons of the ventral nerve cord removed. **b** Null distribution of the silencing effect across the 71 GABAergic cell types making at least 10 synapses onto the nociceptive pathway, plotted against the number of synapses each makes onto the pathway (logarithmic horizontal axis). The dashed line marks the 95th percentile

Decomposition and controls

In a separate run of the decomposition (intact output 29.6 Hz; 107.1 Hz with AN05B004 silenced), removing selectively the synapses of AN05B004 onto afferent terminals changed ascending output to 32.7 Hz, whereas removing only its synapses onto the ascending pathway reproduced almost the entire effect (105.5 Hz). The firing rate of the afferents themselves was essentially unchanged (19.7 to 21.6 Hz) (Online Resource 1, Fig. S4a). The simulated gain change therefore arises from feedforward inhibition of the ascending neurons, not from the axo-axonic synapses, which a point-neuron model driven by forced afferent input cannot represent. When presynaptic inhibition was implemented in its multiplicative form, raising the release factor s from 0.4 to 1.0 increased ascending output 4.5-fold (Online Resource 1, Fig. S4b), indicating that the axo-axonic component would exert a comparable effect if modelled explicitly, although this rests on a modelling assumption rather than on a measured quantity.

A network-instability control distinguished specific disinhibition from network collapse. Under innocuous tactile stimulation, removing all 5,318 VNC GABAergic neurons raised global mean activity 6.5-fold, from 11.7 to 76.4 Hz, whereas removing 5,318 cholinergic neurons reduced it to 7.6 Hz and produced no ascending response (Table 3). Under nociceptive drive, silencing AN05B004 alone raised the ratio of pathway activity to global activity from 4.4 to 17.9, whereas removing all GABAergic neurons reduced it to 1.0 (Table 3; Fig. 8a). An apparent recruitment of the nociceptive pathway by innocuous touch after complete GABAergic loss was therefore attributable to global hyperexcitation rather than to a specific failure of inhibition, and is reported here as a negative control (Online Resource 1, Figs. S2b, S5; Table S5).

Discussion

This is, to the authors' knowledge, the first complete census of axo-axonic inhibitory control of sensory afferents in any nervous system. Three findings emerged. Inhibitory control is

partitioned by sensory modality: the antennal-lobe classes share one inhibitor, and every other afferent class is dominated by a different GABAergic cell type. The partition is enforced synaptically rather than by spatial segregation, since neurons whose arbors contain a large share of a foreign afferent class direct essentially no output to it. And nociceptive afferents are, in all three animals examined, the somatosensory class whose inhibitory control is most concentrated in a single source: in the most completely reconstructed dataset, one bilateral pair of neurons supplies 57% of their total synaptic input, and each of these two neurons is connected with every nociceptor of the abdomen, legs and wings on both sides of the body.

That the method recovers the olfactory case independently, in two connectomes, supports its validity. Presynaptic gain control of olfactory receptor neuron terminals by antennal lobe local interneurons has been established by pharmacology, imaging, receptor knock-down and behaviour (Olsen and Wilson 2008; Root et al. 2008), and here it was recovered from anatomy alone. The nociceptive case has no comparable experimental resolution, which is why the positive control matters.

The architecture described here has a counterpart in the mammalian dorsal horn. In rat lamina I, presynaptic inhibition of C-fibre input is driven by the C-fibres themselves and regulates the degree of primary nociceptive afferent activation needed to excite second-order neurons (Fernandes et al. 2020). AN05B004 implements that arrangement: it receives 54.8% of its input from nociceptive afferents and returns 52.6% of its output to their terminals. What the mammalian work does not provide, because no preparation permits it, is the cellular identity of the interneurons responsible, or the comparison across modalities.

The finding of modality-dedicated inhibitors also bears on an open question about how such circuits are assembled. Betley et al. (2009) reported that GABApre interneurons in mouse spinal cord prefer their sensory target over motor neurons by approximately 2,000 to 1, and that they refuse all substitute targets when the sensory terminal is removed, which they

described as stringent rather than hierarchical recognition. In the same report they noted that the available invertebrate evidence favoured hierarchical recognition, in which removal of a preferred target leads to ectopic synapse formation. The present data show stringent, non-positional target selection in an insect circuit of the same type, which suggests that the distinction is not one between phyla, although connectivity alone cannot show how the selection is achieved during development.

It should be stated plainly that the architecture reported here is not the gate control described by Melzack and Wall (1965). In that model, large-fibre input excites the inhibitory interneuron and closes the gate on nociceptive transmission. AN05B004 receives 54.8% of its input from nociceptive afferents and approximately 0.2% from tactile bristle afferents, which makes the arrangement homotypic negative feedback rather than heterotypic gating, in agreement with the mammalian lamina I result (Fernandes et al. 2020). The distinction matters, because the gate model makes inhibition depend on the balance of large-fibre and small-fibre input (Mendell 2014), whereas homotypic negative feedback depends on the integrity of the inhibitor itself. A heterotypic mechanism of the gate type does exist in the larva, where gentle touch suppresses nociceptor output through GABA-B receptors on nociceptor terminals (Pan et al. 2023). In the adult connectome the dominant inhibitor of the nociceptive terminals is not of this type, although the smaller GABAergic sources could still carry cross-modal signals.

The synapse-level geometry adds a point that the connectivity table alone cannot make. Inhibitory synapses from AN05B004 lie a median of 1.30 μm from the afferent's own output synapses, against 7.32 μm expected by chance, and the reciprocal synapses lie 0.95 μm apart. Presynaptic inhibition acts by reducing transmitter release at the terminal, so its efficacy depends on proximity to the release sites (Rudomin and Schmidt 1999), and the arrangement measured here is the one that mechanism requires. In mouse spinal cord the equivalent

observation was made by immunohistochemistry, where GABApre boutons contact proprioceptive terminals at a mean density of 3.2 boutons per terminal (Betley et al. 2009). The fly arrangement is the same arrangement, measured in a different way and at synaptic resolution.

The organisation of the loop also yields physiological predictions. Because each AN05B004 neuron pools input from every nociceptive afferent and inhibits every nociceptive terminal, the circuit has the architecture of the global gain control of the antennal lobe, where presynaptic inhibition of olfactory receptor neuron terminals scales with the total feedforward input to the lobe (Olsen and Wilson 2008). The corresponding prediction is that noxious stimulation of one part of the body should reduce transmitter release from nociceptors elsewhere, including on the opposite side, so that the ascending signal is normalised by the total nociceptive drive. The receptor machinery for such inhibition is present in these cells. The adult abdominal md neurons are larval class IV neurons that persist through metamorphosis (Jones et al. 2025); in the larva these neurons carry GABA-B receptors near their axon terminals (Pan et al. 2023), and blocking GABA-B receptors, but not GABA-A receptors, enhances their nociceptive responses (Nakamizo-Dojo et al. 2023). In adult leg nociceptors, knock-down of GABA receptors is sufficient to produce allodynia (Khuong et al. 2019). The GABAergic neurons that act on larval nociceptor terminals during cross-modal inhibition have not been identified (Pan et al. 2023), and in the adult the present data nominate AN05B004 as a candidate source. A bilateral inhibitor that serves the whole body is also consistent with the observation that nerve injury on one side of the fly produces hypersensitivity on the opposite, uninjured side (Khuong et al. 2019).

These properties connect the circuit to the natural behaviour of the animal. Activation of the adult abdominal md neurons produces jumping, faster walking and a place avoidance that persists after the stimulus ends, and the ascending neurons that carry these signals reach

premotor circuits for rapid take-off as well as the dopaminergic and mushroom body circuits of learning (Jones et al. 2025). An inhibitor placed at the first synapse of this pathway therefore sets the threshold for both the reflexive escape and the learned avoidance. Global normalisation would compress the overall intensity of nociceptive drive while preserving its relative distribution across afferents, which is the information needed for responses directed at the stimulated site, such as the rolling of larvae towards the stimulated side, which protects them against parasitoid wasps (Hwang et al. 2007), and the grooming directed at the stimulated abdomen in decapitated adults (Jones et al. 2025). Presynaptic feedback at this synapse is also a known site of experience-dependent plasticity: in the larva, noxious experience during development sensitises nociceptor terminals to serotonergic feedback inhibition (Kaneko et al. 2017), and in the adult the magnitude of avoidance increases across repeated stimulation (Jones et al. 2025). Whether AN05B004 takes part in such use-dependent change is directly testable.

The circuit may also be older than the adult. The nociceptors are persisting larval neurons (Jones et al. 2025), and AN05B004, the ascending neurons AN09B018 and ANXXX196 and DNg70 are all annotated as early-born in male-CNS. In the male nerve cord this annotation is assigned from soma position and size and from the calibre of the primary neurite, and the early-born category includes primary neurons, which function in the larva and can survive metamorphosis (Marin et al. 2024). The adult loop could therefore be inherited, at least in part, from the larval nociceptive circuit. A specific parallel supports this possibility. In the larva, GABAergic neurons of the subesophageal zone send descending axons onto nociceptor terminals and suppress their output through GABA-B receptors when a starved animal feeds, so that feeding takes priority over escape (Nakamizo-Dojo et al. 2023). DNg70 is a GABAergic descending neuron of the gnathal ganglia, the adult counterpart of the subesophageal zone, and it inhibits the same pathway in the adult. No larval neuron has yet

been matched to AN05B004 or DNg70, and the annotation of birth time is presumptive, so this remains a hypothesis that the matching of larval and adult neurons could test.

The quantitative asymmetry is the element of this work that transfers. Among the classes surveyed whose input is predominantly GABAergic, the nociceptive class is the only one whose inhibitory control is concentrated in a single source, with the largest single contributor supplying 57% of total input against 3% to 20% for every mechanosensory class. If the same ordering holds in mammals, presynaptic control of nociceptive afferents should prove architecturally less redundant than that of proprioceptive or tactile afferents. This is measurable with existing methods: counting the number of distinct inhibitory sources contacting C-fibre terminals against proprioceptive terminals in the same spinal cord, by volume EM or by labelling of interneuron subtypes, would test it directly. The reagents for such an experiment already exist, since the inhibitory interneuron populations of the dorsal horn are defined molecularly (Hughes et al. 2012; Todd 2017) and the afferent classes to be compared are separable by conduction velocity and by terminal lamina.

Such an asymmetry would offer a structural account of a clinical observation. Loss of spinal GABAergic inhibition after nerve injury produces pain (Moore et al. 2002; Coull et al. 2003; Khuong et al. 2019), and not a proprioceptive deficit of comparable severity, even though proprioceptive afferents receive a larger GABAergic share of their input than nociceptive afferents do (78% to 84% against 67%). A control distributed across dozens of sources tolerates partial loss; a control held by one source does not. The simulations are consistent with this reading: silencing one cell type raised nociceptive pathway output 3.6-fold without disturbing the rest of the network, whereas removing all 5,318 GABAergic neurons of the VNC produced global hyperexcitation in which the signal-to-background ratio of the pathway collapsed.

Three boundaries should be explicit. There is no vertebrate homologue of AN05B004, and what is proposed to transfer is an architectural principle, not a cellular correspondence. *Drosophila* multidendritic afferents are not C-fibres, and the resemblance is functional rather than evolutionary. And what is measured here is nociception, the processing of noxious stimuli; whether the adult fly experiences a state resembling pain is a separate question that connectivity does not address (Jones et al. 2025).

The principal strengths of the study are the completeness of the census, its replication in three independently acquired datasets spanning both sexes, the recovery of an experimentally validated positive control, the independent reproduction of the structural analysis from the written methods alone, the reproduction of the complete pipeline by a computer engineer, and the adversarial review that generated the control analyses.

The work also has important limitations. First, the LIF model does not represent presynaptic inhibition. The simulated gain change arises from feedforward inhibition of the ascending pathway, and the axo-axonic synapses cannot be tested in a point-neuron model whose afferents are driven by forced input. The synapse-localisation analysis partly mitigates this, since it establishes the spatial arrangement the mechanism requires without recourse to the model, but it does not measure its functional strength. Second, alternative interpretations of the connectivity are not excluded by anatomy: dynamic-range compression, adaptation, habituation and suppression of reafference during self-generated movement all remain possible, although only 2.6% of the input to AN05B004 arrives from descending neurons, which weakens an efference-copy account, while 81.6% arrives from sensory afferents. Third, synaptic sign was assigned from neurotransmitter prediction (Eckstein et al. 2024); AN05B004 is predicted to be GABAergic in all three datasets, but the prediction is implausible for several BANC afferents predicted as serotonergic, indicating predictor error in that class. Fourth, the model ignores neuromodulation, gap junctions, dendritic

compartmentalisation and slow GABA-B signalling, and applies a uniform weight per synapse; GABA-B signalling is precisely the mechanism of presynaptic inhibition in the antennal lobe (Olsen and Wilson 2008; Root et al. 2008). Fifth, the 0.275 mV weight was calibrated on a female brain dataset (Shiu et al. 2024), so all effects are reported across the range 0.10 to 0.275 mV. Sixth, whole-CNS runs exclude recurrence between Kenyon cells because it generates runaway activity, a tuning choice which indicates that the model operates near instability. Seventh, each dataset is a single animal with two AN05B004 neurons, so variation between animals of the same sex cannot be assessed. Eighth, the BANC nociceptive class is defined more broadly than in the males, includes digestive-tract afferents and is reconstructed at approximately four-fold lower synapse density, which accounts for its lower concentration index. The BANC abdominal pathway was excluded from simulation because its 43 cholinergic SNch01 neurons make only 14 synapses onto the ascending pathway, and cross-dataset matching of this cell type proved unreliable, with 24 of 68 matched neurons predicted to be serotonergic. Finally, the apparent recruitment of the nociceptive pathway by innocuous touch after complete GABAergic loss was shown by the instability control to reflect network collapse, and is reported as a negative result.

For connectomics, the census is a reusable measurement: the same indices can be computed for any afferent class in any connectome, and the ordering reported here is a prediction that each new dataset tests. For nociception research, AN05B004 is a named cell type whose silencing is predicted to produce thermal and mechanical hypersensitivity without nerve injury, which is directly testable should a driver line that labels it become available. For the mammalian field, the prediction stated above is the main deliverable.

In summary, axo-axonic inhibitory control of primary sensory afferents in the adult *D. melanogaster* CNS is partitioned by sensory modality, and within one developmental hemilineage sibling GABAergic cell types divide the afferent classes between them. The

partition is enforced synaptically rather than by spatial segregation. Nociceptive afferents differ from every other somatosensory class in the concentration of that control: a single bilateral pair of neurons supplies more than half of their total synaptic input and pools nociceptive signals from the whole body, whereas mechanosensory classes distribute the same function across dozens of cell types. This architecture is replicated in three independently acquired connectomes and yields a directly testable prediction for the mammalian dorsal horn, together with a candidate structural account of why loss of spinal inhibition produces pain rather than a proprioceptive deficit of comparable severity.

Supplementary Information

Online Resource 1 (PDF): Figs. S1 to S5 and Tables S1 to S5. Online Resource 2 (ZIP): analysis code, including the independent reimplementation. Online Resource 3 (ZIP): derived census, null-model and simulation tables.

Statements and Declarations

Funding

No funding was received for conducting this study.

Competing interests

The authors declare no competing interests.

Ethics approval

Not applicable. This study used only publicly released connectome datasets and involved no new experiments on animals or humans.

Consent to participate

Not applicable.

Consent to publish

Not applicable.

Data availability

All primary data are publicly available. The male-CNS v1.0 connectome is distributed by Janelia Research Campus at https://male-cns.janelia.org (Berg et al. 2026). MANC v1.2.1 (Takemura et al. 2024) and BANC 888 (Bates et al. 2026) were obtained in harmonised format from the fly connectome data resource at https://github.com/sjcabs/fly_connectome_data_tutorial. Neuron skeletons were obtained from the male-CNS public release. The derived census tables, null-model output and simulation results are provided as Online Resource 3.

Code availability

The analysis code, including the independent reimplementation, is provided as Online Resource 2.

Author contributions

Conceptualization: João Pedro do Couto Caetano, Juliana da Rosa Perez, Artur Ramos Molina; Methodology: João Pedro do Couto Caetano, Artur Ramos Molina; Data curation: Fernanda Silveira Prado; Software: Rodrigo Mendes Rezende; Formal analysis and investigation: João Pedro do Couto Caetano (analyses implemented and executed with the large language models described in Materials and methods, under his supervision), Rodrigo Mendes Rezende; Validation: João Pedro do Couto Caetano, Fátima Caroline dos Santos Welter, Vilson Farias Junior, Rodrigo Mendes Rezende; Visualization: João Pedro do Couto Caetano, Fátima Caroline dos Santos Welter, Vilson Farias Junior; Writing - original draft preparation: João Pedro do Couto Caetano, Juliana da Rosa Perez, Fernanda Silveira Prado; Writing - review and editing: João Pedro do Couto Caetano, Juliana da Rosa Perez, Artur Ramos Molina, Fernanda Silveira Prado, Lucas Damé Simões; Project administration: João Pedro do Couto Caetano, Fátima Caroline dos Santos Welter, Vilson Farias Junior, Artur

Ramos Molina, Fernanda Silveira Prado; Supervision: Lucas Damé Simões. All authors read and approved the final manuscript.

Use of generative artificial intelligence

Large language models were used to implement and execute the analyses, as described in Materials and methods; their output was verified by the authors and reproduced step by step by one of them (R.M.R.). A one-page preliminary document prepared with these models to assess the feasibility of the study was entirely rewritten by the authors. No model is listed as an author. The authors take full responsibility for the content.

References

Bates AS, Phelps JS, Kim M et al (2026) Distributed control circuits across a brain-and-cord connectome. Nature 656:957-970. https://doi.org/10.1038/s41586-026-10735-w

Berg S, Beckett IR, Costa M et al (2026) Sexual dimorphism in the complete *Drosophila* male central nervous system connectome. Cell 189:5504-5526.e15. https://doi.org/10.1016/j.cell.2026.08.015

Betley JN, Wright CVE, Kawaguchi Y, Erdélyi F, Szabó G, Jessell TM, Kaltschmidt JA (2009) Stringent specificity in the construction of a GABAergic presynaptic inhibitory circuit. Cell 139:161-174. https://doi.org/10.1016/j.cell.2009.08.027

Burgos A, Honjo K, Ohyama T et al (2018) Nociceptive interneurons control modular motor pathways to promote escape behavior in *Drosophila*. eLife 7:e26016. https://doi.org/10.7554/eLife.26016

Cheong HSJ, Eichler K, Stürner T et al (2026) Organization of circuits linking descending input to motor output in the Male Adult Nerve Cord connectome. eLife 13:RP96084. https://doi.org/10.7554/eLife.96084

770 Coull JAM, Boudreau D, Bachand K, Prescott SA, Nault F, Sík A, De Koninck P, De
771 Koninck Y (2003) Trans-synaptic shift in anion gradient in spinal lamina I neurons as a
772 mechanism of neuropathic pain. Nature 424:938-942. https://doi.org/10.1038/nature01868
773 Dorkenwald S, Matsliah A, Sterling AR et al (2024) Neuronal wiring diagram of an adult
774 brain. Nature 634:124-138. https://doi.org/10.1038/s41586-024-07558-y
775 Duan B, Cheng L, Bourane S et al (2014) Identification of spinal circuits transmitting and
776 gating mechanical pain. Cell 159:1417-1432. https://doi.org/10.1016/j.cell.2014.11.003
777 Eckstein N, Bates AS, Champion A et al (2024) Neurotransmitter classification from electron
778 microscopy images at synaptic sites in *Drosophila melanogaster*. Cell 187:2574-2594.e23.
779 https://doi.org/10.1016/j.cell.2024.03.016
780 Fernandes EC, Pechincha C, Luz LL, Kokai E, Szucs P, Safronov BV (2020) Primary
781 afferent-driven presynaptic inhibition of C-fiber inputs to spinal lamina I neurons. Prog
782 Neurobiol 188:101786. https://doi.org/10.1016/j.pneurobio.2020.101786
783 Fink AJP, Croce KR, Huang ZJ, Abbott LF, Jessell TM, Azim E (2014) Presynaptic
784 inhibition of spinal sensory feedback ensures smooth movement. Nature 509:43-48.
785 https://doi.org/10.1038/nature13276
786 Hughes DI, Sikander S, Kinnon CM, Boyle KA, Watanabe M, Callister RJ, Graham BA
787 (2012) Morphological, neurochemical and electrophysiological features of parvalbumin-
788 expressing cells: a likely source of axo-axonic inputs in the mouse spinal dorsal horn. J
789 Physiol 590:3927-3951. https://doi.org/10.1113/jphysiol.2012.235655
790 Hwang RY, Zhong L, Xu Y, Johnson T, Zhang F, Deisseroth K, Tracey WD (2007)
791 Nociceptive neurons protect *Drosophila* larvae from parasitoid wasps. Curr Biol 17:2105-
792 2116. https://doi.org/10.1016/j.cub.2007.11.029
793 Im SH, Galko MJ (2012) Pokes, sunburn, and hot sauce: *Drosophila* as an emerging model
794 for the biology of nociception. Dev Dyn 241:16-26. https://doi.org/10.1002/dvdy.22737

795 Jones JM, Sustar A, Mamiya A, Walling-Bell S, Chou GM, Cook AP, Tuthill JC (2025)
796 Ascending nociceptive pathways drive rapid escape and sustained avoidance in adult
797 *Drosophila*. bioRxiv. https://doi.org/10.1101/2025.10.28.684868
798 Jovanic T, Schneider-Mizell CM, Shao M, Masson JB, Denisov G, Fetter RD, Mensh BD,
799 Truman JW, Cardona A, Zlatic M (2016) Competitive disinhibition mediates behavioral
800 choice and sequences in *Drosophila*. Cell 167:858-870.e19.
801 https://doi.org/10.1016/j.cell.2016.09.009
802 Kaneko T, Macara AM, Li R et al (2017) Serotonergic modulation enables pathway-specific
803 plasticity in a developing sensory circuit in *Drosophila*. Neuron 95:623-638.e4.
804 https://doi.org/10.1016/j.neuron.2017.06.034
805 Khuong TM, Wang QP, Manion J, Oyston LJ, Lau MT, Towler H, Lin YQ, Neely GG (2019)
806 Nerve injury drives a heightened state of vigilance and neuropathic sensitization in
807 *Drosophila*. Sci Adv 5:eaaw4099. https://doi.org/10.1126/sciadv.aaw4099
808 Lacin H, Chen HM, Long X, Singer RH, Lee T, Truman JW (2019) Neurotransmitter identity
809 is acquired in a lineage-restricted manner in the *Drosophila* CNS. eLife 8:e43701.
810 https://doi.org/10.7554/eLife.43701
811 Lin A, Yang R, Dorkenwald S et al (2024) Network statistics of the whole-brain connectome
812 of *Drosophila*. Nature 634:153-165. https://doi.org/10.1038/s41586-024-07968-y
813 Mamiya A, Gurung P, Tuthill JC (2018) Neural coding of leg proprioception in *Drosophila*.
814 Neuron 100:636-650.e6. https://doi.org/10.1016/j.neuron.2018.09.009
815 Marin EC, Morris BJ, Stürner T et al (2024) Systematic annotation of a complete adult male
816 *Drosophila* nerve cord connectome reveals principles of functional organisation. eLife
817 13:RP97766. https://doi.org/10.7554/eLife.97766
818 Maslov S, Sneppen K (2002) Specificity and stability in topology of protein networks.
819 Science 296:910-913. https://doi.org/10.1126/science.1065103

820 Melzack R, Wall PD (1965) Pain mechanisms: a new theory. Science 150:971-979.
821 https://doi.org/10.1126/science.150.3699.971
822 Mendell LM (2014) Constructing and deconstructing the gate theory of pain. Pain 155:210-
823 216. https://doi.org/10.1016/j.pain.2013.12.010
824 Moore KA, Kohno T, Karchewski LA, Scholz J, Baba H, Woolf CJ (2002) Partial peripheral
825 nerve injury promotes a selective loss of GABAergic inhibition in the superficial dorsal
826 horn of the spinal cord. J Neurosci 22:6724-6731.
827 https://doi.org/10.1523/JNEUROSCI.22-15-06724.2002
828 Nakamizo-Dojo M, Ishii K, Yoshino J, Tsuji M, Emoto K (2023) Descending GABAergic
829 pathway links brain sugar-sensing to peripheral nociceptive gating in *Drosophila*. Nat
830 Commun 14:6515. https://doi.org/10.1038/s41467-023-42202-9
831 Ohyama T, Schneider-Mizell CM, Fetter RD et al (2015) A multilevel multimodal circuit
832 enhances action selection in *Drosophila*. Nature 520:633-639.
833 https://doi.org/10.1038/nature14297
834 Olsen SR, Wilson RI (2008) Lateral presynaptic inhibition mediates gain control in an
835 olfactory circuit. Nature 452:956-960. https://doi.org/10.1038/nature06864
836 Pan G, Li R, Xu G, Weng S, Yang XL, Yang L, Ye B (2023) Cross-modal modulation gates
837 nociceptive inputs in *Drosophila*. Curr Biol 33:1372-1380.e4.
838 https://doi.org/10.1016/j.cub.2023.02.032
839 Root CM, Masuyama K, Green DS, Enell LE, Nässel DR, Lee CH, Wang JW (2008) A
840 presynaptic gain control mechanism fine-tunes olfactory behavior. Neuron 59:311-321.
841 https://doi.org/10.1016/j.neuron.2008.07.003
842 Rudomin P, Schmidt RF (1999) Presynaptic inhibition in the vertebrate spinal cord revisited.
843 Exp Brain Res 129:1-37. https://doi.org/10.1007/s002210050933

Scheffer LK, Xu CS, Januszewski M et al (2020) A connectome and analysis of the adult *Drosophila* central brain. eLife 9:e57443. https://doi.org/10.7554/eLife.57443

Schlegel P, Yin Y, Bates AS et al (2024) Whole-brain annotation and multi-connectome cell typing of *Drosophila*. Nature 634:139-152. https://doi.org/10.1038/s41586-024-07686-5

Shiu PK, Sterne GR, Spiller N et al (2024) A *Drosophila* computational brain model reveals sensorimotor processing. Nature 634:210-219. https://doi.org/10.1038/s41586-024-07763-9

Takemura SY, Hayworth KJ, Huang GB et al (2024) A connectome of the male *Drosophila* ventral nerve cord. eLife 13:RP97769. https://doi.org/10.7554/eLife.97769

Todd AJ (2017) Identifying functional populations among the interneurons in laminae I-III of the spinal dorsal horn. Mol Pain 13:1744806917693003. https://doi.org/10.1177/1744806917693003

Tracey WD, Wilson RI, Laurent G, Benzer S (2003) *painless*, a *Drosophila* gene essential for nociception. Cell 113:261-273. https://doi.org/10.1016/s0092-8674(03)00272-1

Tuthill JC, Wilson RI (2016) Mechanosensation and adaptive motor control in insects. Curr Biol 26:R1022-R1038. https://doi.org/10.1016/j.cub.2016.06.070

Varshney LR, Chen BL, Paniagua E, Hall DH, Chklovskii DB (2011) Structural properties of the *Caenorhabditis elegans* neuronal network. PLoS Comput Biol 7:e1001066. https://doi.org/10.1371/journal.pcbi.1001066

White JG, Southgate E, Thomson JN, Brenner S (1986) The structure of the nervous system of the nematode *Caenorhabditis elegans*. Philos Trans R Soc Lond B Biol Sci 314:1-340. https://doi.org/10.1098/rstb.1986.0056

Winding M, Pedigo BD, Barnes CL et al (2023) The connectome of an insect brain. Science 379:eadd9330. https://doi.org/10.1126/science.add9330

Supplementary Files

This is a list of supplementary files associated with this preprint. Click to download.

- ESM2.zip
- ESM3.zip
- ESM1.pdf